Optical Engineering

SPIEDigitalLibrary.org/oe

Swing arm optical coordinate-measuring machine: high precision measuring ground aspheric surfaces using a laser triangulation probe

Yuhao Wang
Peng Su
Robert E. Parks
Chang Jin Oh
James H. Burge

Swing arm optical coordinate-measuring machine: high precision measuring ground aspheric surfaces using a laser triangulation probe

Yuhao Wang
Peng Su
Robert E. Parks
Chang Jin Oh
James H. Burge
University of Arizona
College of Optical Sciences
1630 E. University Boulevard
Tucson, Arizona 85721
E-mail: psu@optics.arizona.edu

Abstract. The swing arm optical coordinate-measuring machine (SOC), a profilometer with a distance measuring interferometric sensor for in situ measurement of the topography of aspheric surfaces, has shown a precision rivaling the full aperture interferometric test. To further increase optical manufacturing efficiency, we enhance the SOC with an optical laser triangulation sensor for measuring test surfaces in their ground state before polishing. The calibrated sensor has good linearity and is insensitive to the angular variations of the surfaces under testing. Sensor working parameters such as sensor tip location, projection beam angle, and measurement direction are calibrated and incorporated in the SOC data reduction software to relate the sensor readout with the test surface sag. Experimental results show that the SOC with the triangulation sensor can measure aspheric ground surfaces with an accuracy of 100 nm rms or better. [DOI: 10.1117/1.OE.51.7.073603]

Subject terms: swing arm profilometer; profilometry; aspherics; optical testing; laser triangulation sensor; ground surface metrology.

Paper 120473 received Mar. 30, 2012; revised manuscript received May 16, 2012; accepted for publication May 30, 2012; published online Jul. 6, 2012.

1 Introduction

In the field of optical metrology for aspheric optics fabrication, most of the interferometric tests (visible spectrum range) that provide high-accuracy measurement are used after the test surface is polished. But at the polishing stage, the surface shape, or figure, correction is slow. It is desirable to measure the surface accurately during grinding to minimize figure errors and speed up fabrication.

Different techniques have been developed for testing ground surfaces. One traditional method is to use an infrared interferometer. However, as with visible interferometers, null optics are needed for measuring the aspheric shape. The design and alignment of the null optics are complex and time consuming. The limited infrared material choices and the nonvisible light make the use of the infrared interferometer even more difficult.

A laser tracker or laser tracker plus system[1] such as the one used for the Giant Magellan Telescope primary mirror segment is another way to measure a mirror during grinding. The basic idea uses a commercial laser tracker system with the spherically mounted retroreflector (SMR) touching the mirror surface. Since it is a point by point test, it takes time to collect a large number of samples.

There is a new prototype called SLOTS[2] based on reflection deflectometry using a long-wave infrared source scanning technique to measure the surface slope variation of ground surfaces. It is a simple, fast, low-cost, and non-null system that can measure surface slopes to microradian precision. The method is promising but needs further development.

The swing arm optical CMM (SOC),[3–5] developed at the University of Arizona, is a profilometer with a distance measuring interferometric sensor. It is used for *in situ* measurement of highly aspheric mirrors, and it has shown a performance rivaling full aperture interferometric tests. The interferometric sensor has high precision and a high data rate, but it only works for polished surfaces. A contact sensor, with a linear variable differential transformer (LVDT), has been used with the SOC to measure ground surfaces, but the measurement is time consuming, because the probe is picked up after each point to avoid scratching the surface.

Different types of sensors have been studied for ground surface metrology. There are some sensors based on the confocal principle[6] with linearity at the submicron level. There are sensors based on laser triangulation that have a resolution of 10 nm and are insensitive to surface angular variation. The triangular sensors work on both polished and ground surfaces and were chosen and calibrated[7] for use in our application. The laser triangulation technique has been used for many applications, such as inspection of free-form surfaces[8,9] and blind guidance.[10] The measurement uncertainty due to speckle noise, the test lateral resolution, and the aspect of the test sensitivity to the surface texture distribution have been investigated.[11–13] For high-precision optical surface measurement applications like astronomical telescope mirror metrology, the only work reported are some simulations showing the potential measuring accuracy using different types of triangulation sensors.[14,15]

This paper shows the results of calibrating a triangulation sensor and using it to measure large ground mirrors. The paper is organized as follows: In Sec. 2, we review the basic principle of the SOC and laser triangulation sensors.

In Sec. 3, we describe the calibration of a triangulation sensor and show some metrology results compared to an interferometric null test of a highly aspheric mirror. Finally, conclusions are drawn in Sec. 4.

2 Principles

2.1 *Principle of the SOC*

The basic geometry of the swing-arm profilometer is shown in Fig. 1. A sensor is mounted at the end of an arm that swings across the optic under test such that the axis of rotation of the arm goes through the center of curvature of the optic. The arc defined by the sensor tip trajectory, for a constant sensor reading, lies on a spherical surface defined by this center of curvature. For measuring aspheric surfaces, the sensor that is aligned parallel to the normal to the optical surface at its vertex reads only the surface departure from spherical. The SOC uses this simple geometry with an optical, noncontact, interferometric sensor that measures continuously across the optic. The optic or test part is rotated in azimuth after each profile is measured. Figure 2 shows an example of the profiling pattern we generally use during a test. Since the arcs cross each other while the sensor scans the mirror edge to edge, we know the surface heights must be the same at these scan crossings. The crossing height information is used to stitch the profiles into a surface using a maximum likelihood reconstruction method.[3,16,17] Figure 3 shows the results of using the SOC and a full aperture interferometric null test to measure a 1.4-m diameter aspheric surface that has an aspheric departure of 300 μm. The SOC test shows excellent agreement with the interferometric test. The direct subtraction of the maps from the two methods, after alignment terms have been removed, shows a difference of only 9 nm rms, much of which appears to come from the interferometric test.

2.2 *Principle of the Laser Triangulation Sensor*

Laser triangulation is widely used in various applications to measure distances to objects. A common triangulation principle is to project a light spot on to the object and extract the distance information from the reflected or scattered light.[14]

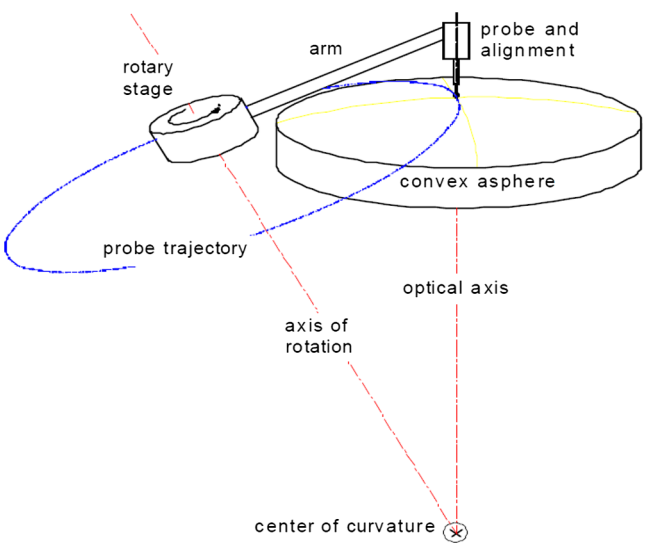

Fig. 1 Basic geometry of the swing-arm profilometer.

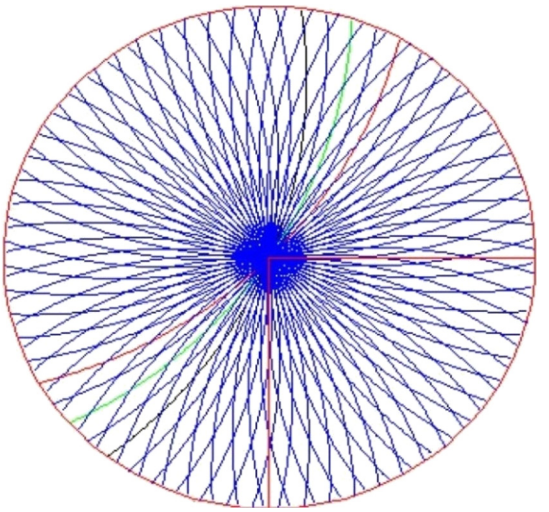

Fig. 2 An example of the SOC profiling pattern.

High measuring rates, high spatial resolution, large measuring range, and zero applied force are significant advantages of the laser triangulation sensor over other types of distance measuring sensors.

There are two types of triangulation sensors normally used. The first one is an orthogonal sensor, in which the output plane is perpendicular to its optical axis. The second one has a tilted sensor, in which the output plane is tilted according to the Scheimpflug principle. Tilting of the output plane eliminates defocus and makes the sensor insensitive to the angular variations of the test surface due to the imaging effects.[14] The sensor investigated and used on the SOC is the second type.

The geometry of the sensor measuring method is shown in Fig. 4. The incident beam with angle θ hits the surface at the sensor's tip position O, where the sensor reads zero, and then reflects or scatters back and passes through an imaging lens inside the sensor. Finally, the beam falls on the detector of the sensor. The measuring axis is the bisector of the incident and reflected beam. By knowing the spot tip position and incident beam angle, we can trace the ray to O' when the surface moves up to $S2$. The ray will reflect or scatter at the surface and be collected by the imaging lens if the distance d is within the sensor's dynamic range. The sensor's detector plane is tilted and is conjugate with the OO' plane according to the Scheimpflug principle. The difference of the spot positions is a function of the displacement d, the projection beam angle, the magnification of the optical system, and the focal length of the imaging lens as described by Mikhlyaev.[14] The commercial triangulation sensor is usually calibrated so that the output signal is linear with the test surface displacement.

3 Calibration

The sensor's linearity, angular sensitivity, and scaling effect were measured experimentally. The zero position (tip position) of the sensor projected beam, the direction of the projected beam, and the measurement axis were calibrated and used as the input for the SOC data reduction. Finally, the system performance with the triangulation sensor was verified by measuring test surfaces with known shapes. The flow chart in Fig. 5 shows the outline of the calibration steps.

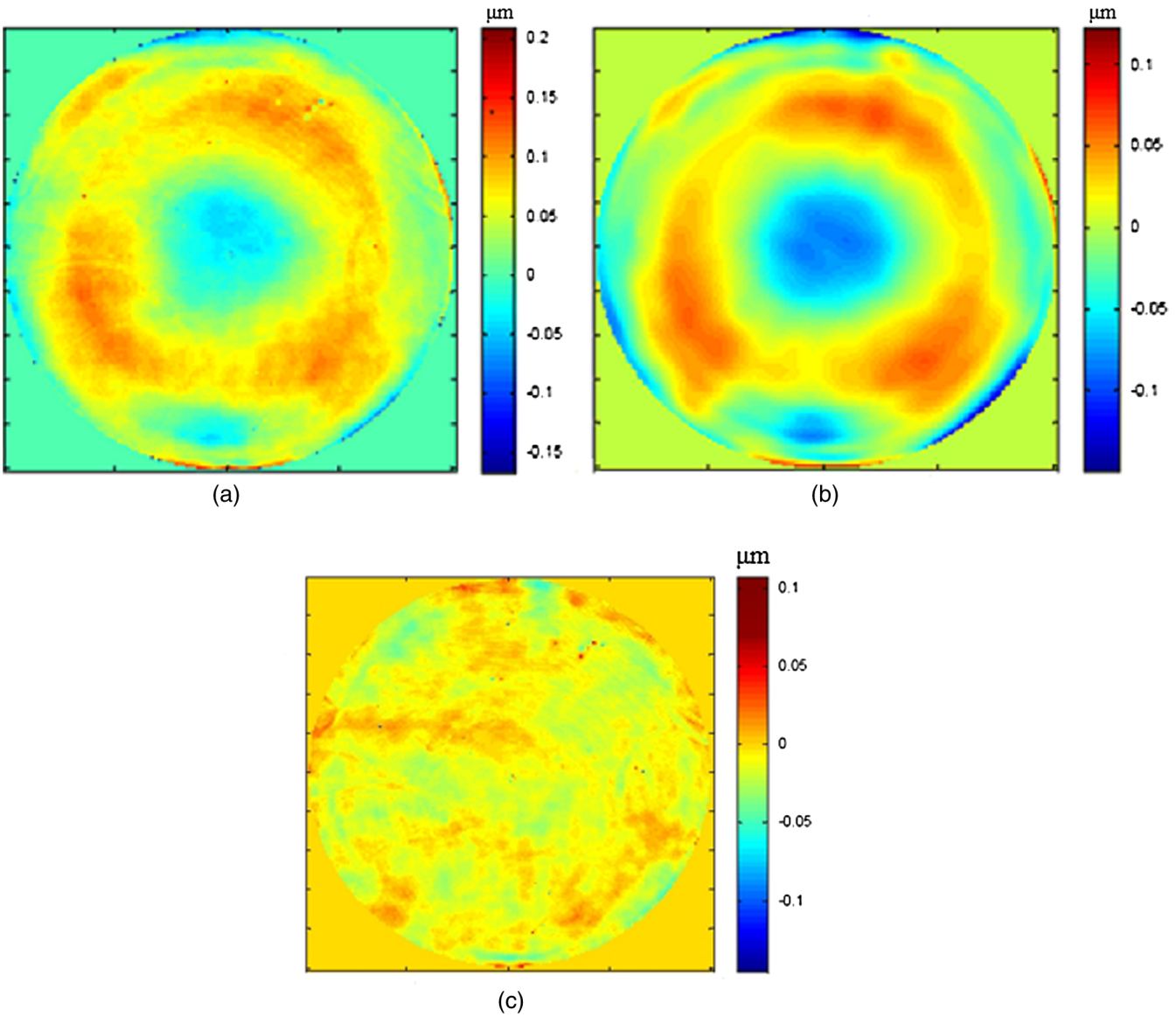

Fig. 3 Comparison of the interferometric Fizeau test data (a) and the SOC data (b) with tilt, power, coma, astigmatism, and trefoil removed. In the Fizeau test, rms = 0.0357 μm. In the SOC, rms = 0.0356 μm. (c) Direct subtraction shows a difference of 9 nm rms, much of which appears to come from the interferometric test.

3.1 *Linearity*

A distance measuring interferometer (DMI)[18] was used to check the linearity of the triangulation sensor. The DMI has accuracy at nanometer level. The setup is shown in Fig. 6. The DMI and the triangulation sensor were aligned to be able to measure simultaneously the motion from a double-sided flat mirror, which was mounted on a flexure. The flexure was driven with a voice coil and function generator to oscillate sinusoidally with a peak-valley motion of 2 mm at a frequency of a few Hz. One side of the

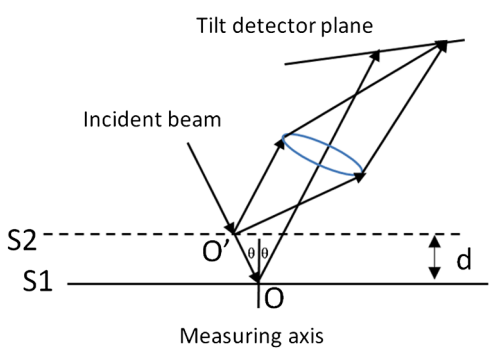

Fig. 4 Measurement principle of the triangulation sensor.

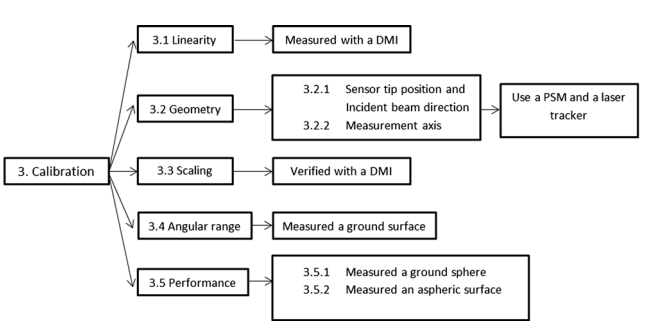

Fig. 5 Outline of the calibration steps for the triangulation sesnor.

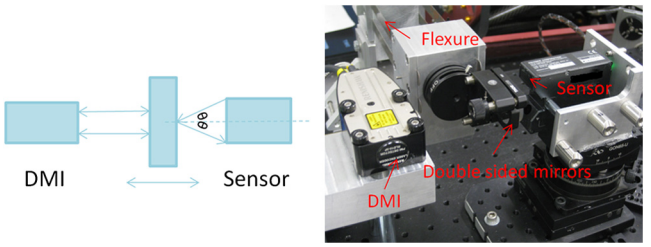

Fig. 6 Calibration of the triangulation sensor's linearity with a distance measuring interferometer.

double-sided flat mirror was specular as the target for the DMI, while the other side of the flat was ground for evaluating the triangulation sensor.

We budgeted a signal difference of 10 nm or less from the test system alignment and the motion effect. (The sensor has a 10 nm resolution.) The motion of the flexure with the flat mirror was designed and checked with an alignment telescope to show an angular variation of a few arc-seconds. The DMI and the triangulation sensor are aligned to each other to minimize the cosine errors and Abbe errors.

Figure 7 shows an example of the signals obtained from the DMI and the triangulation sensor. The readout difference from the direct subtraction of the DMI and triangulation sensor data was ~60 nm rms as shown in Fig. 8. The difference was dominated by the random noise from the environment and the ground mirror surface roughness, because the incident beam from the triangulation sensor moves across the mirror as it is oscillated. Later we show that when the sensor is mounted on SOC and tests a polished surface, a precision of 20 nm rms is achieved when an average of eight single measurements is used.

3.2 *Calibration of the Geometry of the Sensor*

3.2.1 *Sensor tip location and the direction of the projected beam*

When measuring a test surface, as seen in Fig. 9, the coordinates of the point of measurement are a function of the

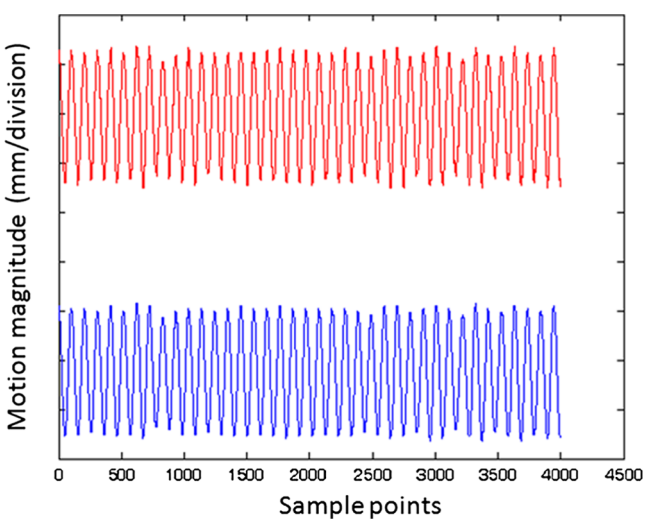

Fig. 7 Data readout from the DMI (upper) and the triangulation senor (lower), using about 4,000 sampling points and 2 mm sinusoidal motion.

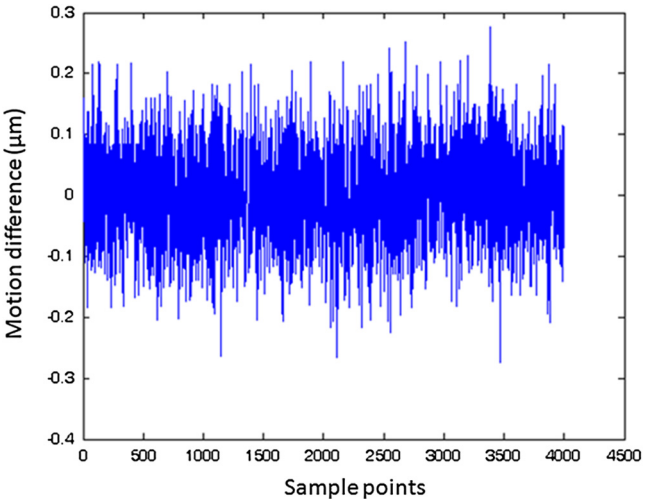

Fig. 8 Readout difference between the DMI and the triangulation senor (rms = 0.06 μm).

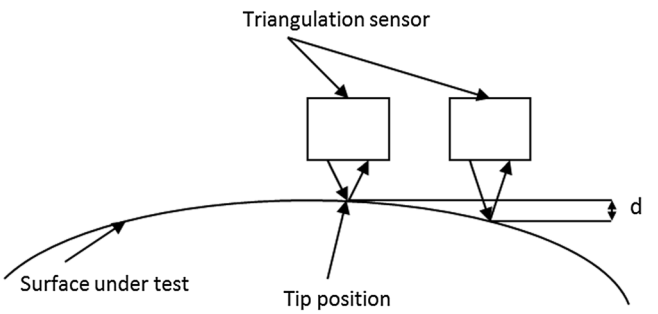

Fig. 9 The coordinates of the point of measurement and the angular dynamic range of the triangulation sensor.

sensor position, the direction of the projected light beam relative to the surface, and the test surface shape. Following the SOC coordinate calibration concept described by Su et al.,[4,5] we calibrated the relationship between the sensor nominal tip position when the sensor reads zero and the direction of the projected light beam relative to reference features on the sensor case, namely, three laser tracker spherically mounted retroreflectors (SMRs). When the sensor is installed on the SOC, the coordinate relationship is used to determine the sensor tip location and angle of the projected beam relative to the surface under testing. This is done by measuring the three SMRs' locations with a laser tracker. Then at each scan position, the coordinates of the point of measurement on the test surface can be calculated with a simple ray tracing algorithm in the SOC data reduction code.

To perform the calibration, we used a point source microscope (PSM)[19] and a laser tracker.[20] As shown in Fig. 10, a piece of 25-μm thick translucent shim stock was located between the sensor and the PSM. The shim stock was positioned normal to the sensor's measuring axis. The sensor was mounted on an x, y, z stage that brought the sensor up to the shim stock until the sensor read zero. Then a PSM was brought up to focus on the backside of the shim stock, so the PSM was focused on the effective sensor measuring spot as seen through the shim stock. When the sensor and the PSM were in these positions, the locations of the three SMRs on the sensor were measured with the laser

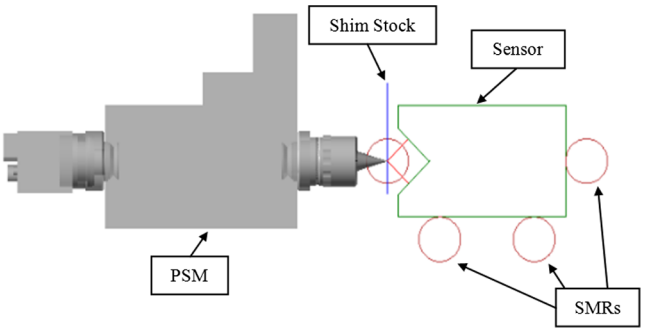

Fig. 10 Schematic picture of the triangulation sensor coordinate point of measurement calibration.

tracker. Then the sensor was moved out of the way, and the center of a solid steel ball was positioned at the focus of the PSM objective. Then the solid ball was removed from the SMR nest and replaced with an SMR. The SMR was measured with the laser tracker as shown in Fig. 11. Now the laser tracker has information about the measuring spot location at the zero height reading of the sensor relative to the SMR nests on the sensor. By moving the shim stock to different sensor height locations of the projected beam and repeating the above procedures, several locations along the projected beam were measured, and the direction of the projection beam was determined. The thickness of the shim stock was backed out during the data processing. The accuracy of the calibration in terms of the SOC coordinates was determined to a few microns.

3.2.2 *Sensor measurement axis*

The readout of the sensor is the displacement d along the axis of the sensor as shown in Fig. 9. Thus it is important to calibrate the sensor measurement direction relative to the sensor axis and align the sensor axis to the SOC test system. This calibration was initially done using the setup in Fig. 6. After the DMI and the triangulation sensor were aligned to minimize the readout difference between the two sensors, we used a laser tracker to measure the three SMRs' locations on the sensor. Then the double-sided flat mirror and the sensor were removed, and a reference flat mirror was put far from the DMI but normal to the DMI beam as shown in Fig. 12. We used a tracker ball touching the mirror surface to find the mirror surface normal. The sensor's measuring axis was parallel to the DMI axis and the mirror surface normal. The projected angle θ shown in Fig. 6 can be calculated from these results and the direction of the projected beam.

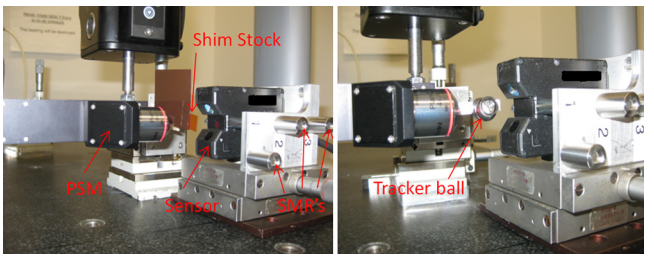

Fig. 11 Experimental setup for determining the measurement spot location and projected beam direction.

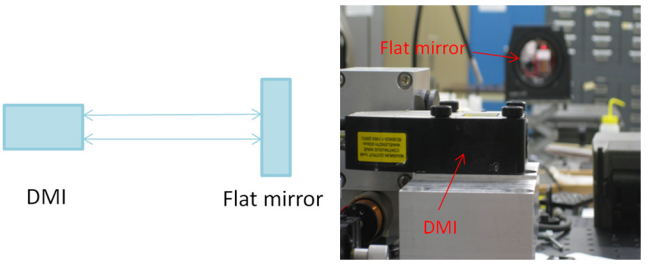

Fig. 12 Calibration of the measurement axis of the sensor.

3.3 *Scaling Effect*

A scaling factor is introduced if the sensor is tilted relative to the test surface. As seen from Eq. (1), the scaling factor can be derived from the triangulation sensor test geometry. The scaling sensitivity was tested by tilting the sensor relative to the double-sided flat as shown from Fig. 13.

$$\text{Scaling factor} = 1/\cos(\theta) - 1/\cos(\theta \pm \varphi). \tag{1}$$

In Fig. 13, θ is the beam projection angle, and φ is in the plane of rotation angle of the sensor. (The sensor readout is insensitive to the out-plane rotations for small angles.) This scaling effect needs to be taken into account during the SOC alignment to the test part. It has a sensitivity of $\sim 0.015/$ deg for the particular sensor we used. As the test surface aspheric departure gets larger, the scaling effect from the sensor angular alignment becomes more significant. For instance a test surface with a 2 mm peak-valley aspheric departure and with 0.01 deg alignment errors will have scaling induced errors up to 0.3 μm in P-V. This scaling sensitivity puts a long-term stability requirement on the SOC. The test triangulation sensor system is sensitive to the angular drift between the sensor and the test surface.

As seen from Eq. (1), the projection angle can also be checked by varying some known angles between the sensor and the double-sided mirror and then reading out the scaling factor from the difference between the sensor and the DMI readings.

3.4 *Angular Dynamic Range*

A large angular working range from the sensor is desired, as we would like the sensor to continue to work when the test surface normal is not parallel to the measurement axis of the sensor. This is the situation for the SOC when the surface has a large departure from a sphere or a flat. As seen from Fig. 9, we need to know the angular range over which the sensor reads out the surface sag d, independent of the slope of the surface. The triangulation sensor we are using has the property that the detector plane is conjugate with the testing location, which is along the line of the projected beam as

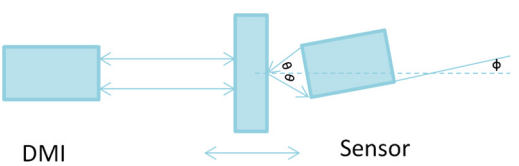

Fig. 13 Calibration of triangulation sensor's scaling factor with a distance measuring interferometer.

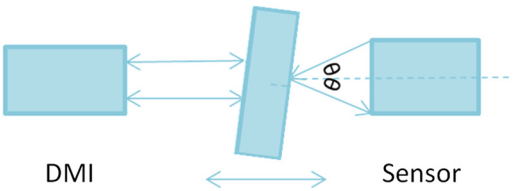

Fig. 14 A possible experimental layout to test the sensor angular dynamic range based on the existing setup.

shown in Fig. 4. Due to this imaging relationship, the sensor is insensitive to the local slope variations of the test surface.

A possible experiment layout for testing the sensor angular range based on the existing setup is shown in Fig. 14. However, the angular range of the DMI is only a few minutes of arc and cannot support the large angular range we would like to investigate.

Another approach might be using a wedged double-sided mirror. However, multiple samples would be needed for sampling the angular range we are interested in, and the sampling is not continuous.

Instead, we decided to test the angular range by measuring a ground optical surface with a known shape as described below. The results show that the sensor maintains good linearity over the angular range tested of about ± 3 deg.

3.5 *System Calibration*

3.5.1 *Calibration under a CMM with a ground spherical surface*

The initial system test was done using a CMM as the scanning device before the sensor was verified for service on the SOC as shown in Fig. 15. The x and y linear stages of the CMM were used to scan and record the coordinates of the mirror under testing. (The coordinates were further corrected with ray tracing.) The CMM z axis was locked, and the surface sag was read out by the sensor. A spherical convex ground surface was measured for calibration. The radius of curvature and diameter of the sample mirror was chosen so that the 2 mm sensor working range and a ± 3 deg angular range could be checked by scanning the full aperture of the mirror.

The data were collected continuously along the x axis for different y values using the CMM. Figure 16 shows an example of the data obtained from the scans. Each line in the figure corresponds to a particular x scan with a fixed y value. This shows the sag value seen by the sensor relative to the angle between the sensor axis and the normal to the sphere being tested. The performance of the sensor for different working angles is checked by this sampling strategy.

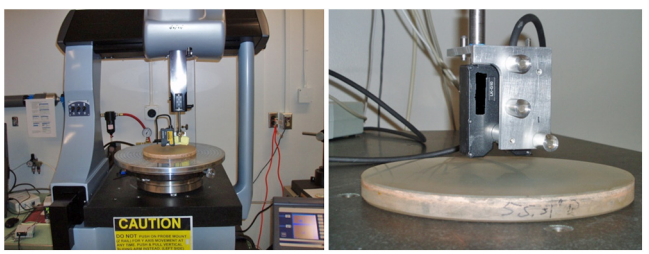

Fig. 15 Calibration of the triangulation sensor with a ground convex spherical mirror.

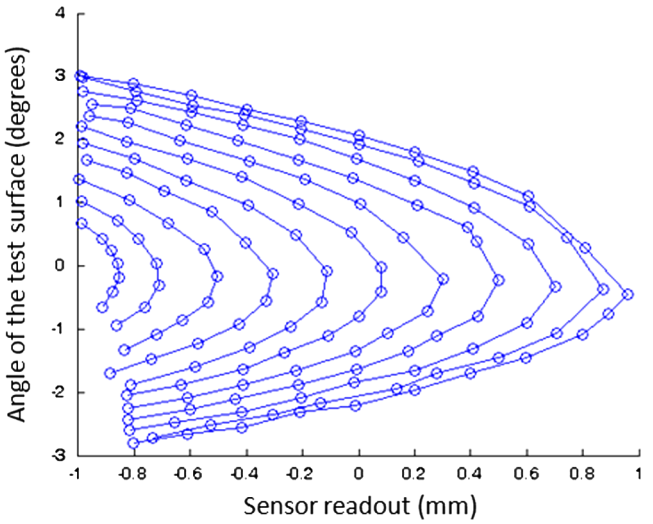

Fig. 16 Example output from the CMM scans that gives the sag value relative to the angle seen by the sensor.

The setup offered a simple way of collecting a large number of data points rather quickly. In addition, it was easy to calculate the theoretical sag of the sphere at each point to compare with the measured values. After removing the ideal spherical shape, the difference map in Fig. 17 shows an rms difference of 0.62 μm. The errors are dominated by the scanning errors from the CMM rails, the deflection of the sensor due to moments induced by the readout cable, and the ground surface roughness. No systematic errors due to sensor angular dynamic range issues were noticed.

3.5.2 *Measuring an aspheric surface*

To check the system performance, we attached the calibrated sensor to the SOC to guide the grinding of a 1-m diameter 80 μm P-V aspheric surface. Figure 18 shows the comparison of the measurements from the SOC and from a null interferometric test when the mirror was in its polishing stage. The results show the SOC and interferometer data agree with

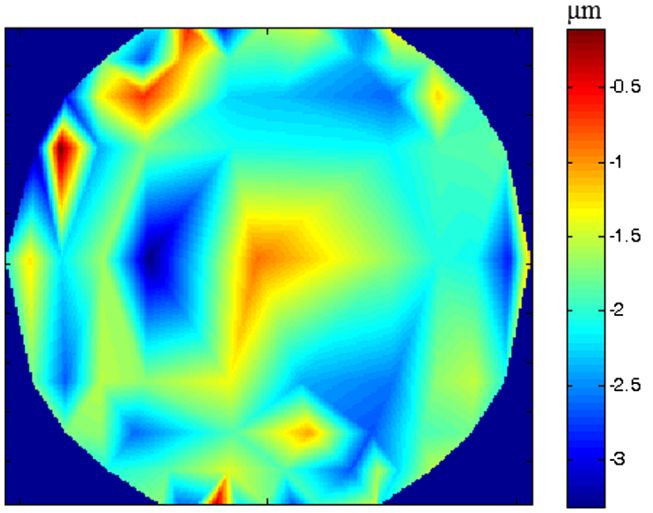

Fig. 17 Difference between the measured and ideal surface for a convex ground surface (rms = 0.062 μm).

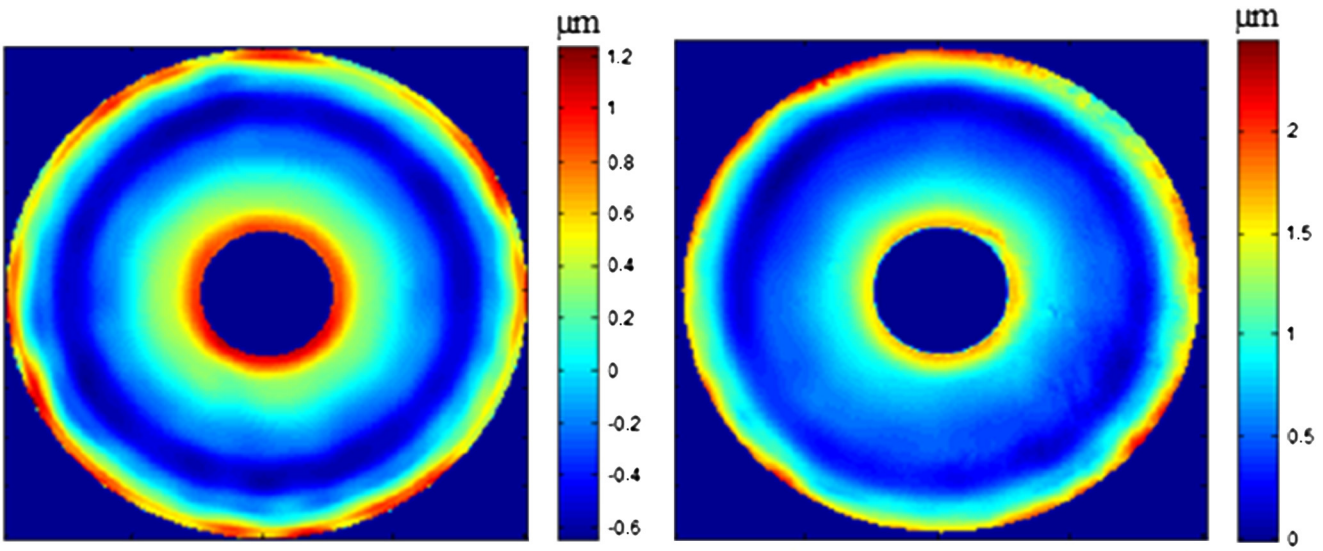

Fig. 18 Measurement of a highly aspheric surface with (a) the SOC (surface map with power, astigmatism, coma, and trefoil removed), where rms = 0.41 μm and (b) the null interferometric test, where rms = 0.44 μm.

each other to 100 nm rms or better. This shows that the triangulation sensor is reliable for measuring both ground and polished surfaces.

4 Conclusion

The SOC is an important metrology technique for highly aspheric surface testing because of its versatility and high accuracy. It is configurable for measuring concave, convex, and plano surfaces. It can make *in situ* measurements, and its high-precision performance can rival full aperture interferometric tests. We have shown how the measurement range of the SOC can be extended to ground surfaces by using a calibrated laser triangulation sensor, and we have shown how to carry out that calibration. The experimental data show that the SOC equipped with a triangulation sensor can measure a test surface to a precision of better than 100 nm rms. This significantly improves the optical fabrication efficiency by extending precision metrology into the grinding cycle of the fabrication.

References

1. T. L. Zobrist et al., "Measurements of large optical surfaces with a laser tracker," *Proc. SPIE* **7018**, 70183U (2008).
2. T. Su et al., "Scanning long-wave optical test system: a new ground optical surface slope test system," *Proc. SPIE* **8126**, 81260E (2011).
3. P. Su et al., "Swing arm optical CMM for aspherics," *Proc. SPIE* **7426**, 74260J (2009).
4. P. Su et al., "Swing arm optical coordinate-measuring machine: modal estimation of systematic errors from dual probe shear measurements," *Opt. Eng.* **51**(4), 043604 (2012).
5. P. Su et al., "Swing arm Optical CMM: self calibration with dual probe shear test," accepted to *Proc. SPIE* **8126**, 81260W (2011).
6. Acuity laser measurement, "White light confocal displacement sensor," 043604 (Nov 2010) http://doc.diytrade.com/docdvr/1391688/21942722/1308161289.pdf.
7. Keyence America, "High-speed, high-accuracy CCD laser displacement sensor," Keyence America (2012) http://www.keyence.com/products/measure/laser/lkg/lkg.php, http://www.micro-epsilon.com/displacement-position-sensors/laser-sensor/index.html.
8. N. Van Gestel et al., "A performance evaluation test for laser line scanners on CMMs," *Optic. Laser. Eng.* **47**, 336–342 (2009).
9. B. Muralikrishnan et al., "Dimensional metrology of bipolar fuel cell plates using laser spot triangulation probes," *Meas. Sci. Technol.* **22**, 075102 (2011).
10. J.-H. Wu et al., "The application of laser triangulation method on the blind guidance," *Proc. SPIE* **8133**, 81330V (2011).
11. R. G. Dorsch, G. Häusler, and J. M. Herrmann, "Laser triangulation: fundamental uncertainty in distance measurement," *Appl. Optic.* **33**, 1306–1314 (1994).
12. D. MacKinnon et al., "Lateral resolution challenges for triangulation-based three dimensional imaging systems," *Opt. Eng.* **51**, 021111 (2012).
13. M. Daneshpanah and K. Harding, "Surface sensitivity reduction in laser triangulation sensors," *Proc. SPIE* **8133**, 81330O (2011).
14. S. V. Mikhlyaev, "High-precision triangulation sensing of mirror surface," *Proc. SPIE* **4416**, 400–403 (2001).
15. S. V. Mikhlyaev, "Influence of a tilt of mirror surface on the measurement accuracy of laser triangulation rangefinder," *J. Phys. Conf.* **48**, 739–744 (2006).
16. P. Su et al., "Maximum likelihood estimation as a general method of combining sub-aperture data for interferometric testing," *Proc. SPIE* **6342**, 63421X (2007).
17. P. Su, J. H. Burge, and R. E. Parks, "Application of maximum likelihood reconstruction of sub-aperture data for measurement of large flat mirrors," *Appl. Optic.* **49**(1), 21–31 (2010).
18. Renishaw, "RLE system overview," (2012) http://www.renishaw.com/en/rle-system-overview--6594.
19. R. E. Parks and W. P. Kuhn, "Optical alignment using the point source microscope," *Proc. SPIE* **5877**, 58770B (2005).
20. J. H. Burge et al., "Use of a commercial laser tracker for optical alignment," *Proc. SPIE* **6676**, 66760E (2007).

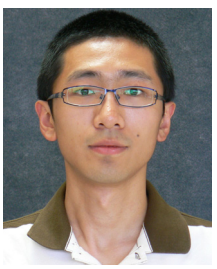

Yuhao Wang received his BS in engineering from Changchun University of Science and Technology in 2009. He is currently a PhD student at the College of Optical Sciences at the University of Arizona. As a research assistant, he is working on developing new optical testing techniques. His research interests include optical metrology.

Peng Su received his BS and MS in optics from Beijing Institute of Technology and his PhD in optical sciences from the University of Arizona. His current research focuses on developing advanced technologies for optical testing of large optical components and systems. The technologies he developed include a swing-arm optical-coordinate-measuring machine for highly aspheric surfaces, a scanning pentaprism test for off-axis paraboloidal mirrors, a software configurable optical test system (SCOTS) for free-form surfaces, and a maximum-likelihood method for meter level large flat stitching and self-calibration.

Robert E. Parks received his BA and MA in physics from Ohio Wesleyan University and Williams College, respectively. He then worked as an optical engineer at Eastman Kodak Company and Itek Corporation prior to gaining optical fabrication experience at Frank Cooke, Inc. In 1976, he went to the Optical Sciences Center at the University of Arizona as manager of the optical shop and was subsequently promoted to assistant research professor. In 1992, he started Optical Perspectives Group, LLC, along with Wm. P. Kuhn, and continues to operate the business while working part-time at the College of Optical Sciences.

Chang Jin Oh received his BS in engineering mechanics from Chungbuk National University in 1994 and his MS and PhD in mechanical engineering in 1996 and 2003, respectively, from Chungbuk National University in South Korea. He joined the College of Optical Sciences at the University of Arizona in 2004, and his current position is senior scientist in optomechanics at the University of Arizona. His interests are optical fabrication, testing, and optomechanics.

James H. Burge received his BS in engineering physics from Ohio State University in 1987 and his MS and PhD in optical sciences in 1991 and 1993, respectively, from the University of Arizona. His current position is professor at the University of Arizona with joint appointments in optical sciences and astronomy. His interests are astronomical optics, optical fabrication and testing, optomechanics, and optical system engineering.